arXiv:cond-mat/0511316v2 [cond-mat.supr-con] 15 Nov 2005

Charge-Inhomogeneity doping relations in $YBa_2Cu_3O_y$ detected by Angle Dependent Nuclear Quadrupole Resonance

Rinat Ofer, Shahar Levy, Amit Kanigel, and Amit Keren
Department of Physics, Technion - Israel Institute of Technology, Haifa 32000, Israel.

The origin of charge inhomogeneity in $YBa_2Cu_3O_y$ is investigated using a new experimental method designed to determine the nuclear quadrupole resonance (NQR) asymmetry parameter η for very wide NQR lines at different positions on the line. The method is based on the measurement of the echo intensity as a function of the angle between the radio frequency field $\mathbf{H}_1$ and the principal axis of the electric field gradient. Static charge inhomogeneity deduced from $\eta > 0$ are found in this compound, but *only* in conjunction with oxygen deficiency. This limits considerably the possible forms of charge inhomogeneity in bulk $YBa_2Cu_3O_y$.

The discussion on the mechanism for high temperature superconductivity (HTSC) is focused these days on the presence or absence of charge and spin inhomogeneity in the CuO_2 planes. Such inhomogeneity can lead to a one dimensional boundary, possibly in the form of stripes, between "hole-rich" and "hole-poor" regions and, allegedly, to superconductivity.[1] Indeed, it is now established by both surface and bulk techniques that most of the underdoped cuprates phase separate into "hole-rich" and "hole-poor" regions. For example, there is a consensus derived from surface sensitive STM experiments [2] on underdoped $Bi_2Sr_2CaCu_2O_{8+\delta}$ that the planes are inhomogeneous. A different example is $La_{2-x}Sr_xCu_1O_4$ [LSCO] where the evidence for phase separation is derived from experiments sensitive to both magnetic fluctuation, such as muon spin relaxation (μSR) [3], and charge fluctuations such as nuclear quadrupole resonance (NQR).[4] Even in very underdoped $YBa_2Cu_3O_y$ ($YBCO_y$) phase separation is observed; neutron scattering from phonons related to charge inhomogeneity is found in doping levels up to $YBCO_{6.35}$ [5], and μSR detects a spin glass phase for a similar doping range.[6] However, the origin of this phase separation is still not clear; is it coming from competing phases in the CuO_2 plane, or does it simply stem from the quenched disorder introduced by doping?

A possible way to address this question is to apply NQR to $YBCO_y$ since in this compound one can distinguish between different in-plane coppers [Cu(2)] resonance lines, and associate each line with a local environment. However, a standard NQR based determination of charge homogeneity is not available to date due to the complicated and very wide spectrum of underdoped YBCO (which will be reviewed below). The purpose of this work is to overcome the NQR problems and to shed light on the evolution of charge homogeneity in the bulk of YBCO close to optimal doping. For this purpose we developed a new experimental technique based on the measurement of the Cu(2) NQR echo intensity as a function of the angle between the radio frequency (RF) field, $\mathbf{H}_1$, and the principal axis of the electric field gradient (EFG) at the copper site. We call this angle-dependent NQR technique ADNQR.

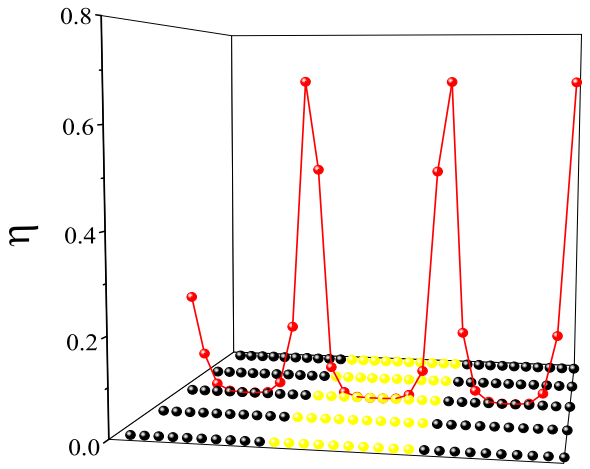

FIG. 1: (Color online) A toy model calculation for $|\eta|$ in the presence of charge stripes in the CuO_2 plane. See text for details.

Standard NQR is based on the fact that nuclei with spin $I > 1/2$ can be viewed as positively charged oval objects. As a result, their energy inside a solid depends on their orientation in the electrostatic potential $V(\mathbf{r})$ generated by the other nuclear and electronic charges. When the nuclear poles are close to positive charges their energy is high, and when the poles are close to negative charges the energy is low. The energy difference between different orientations is determined by the EFG tensor $V_{ij} = \frac{\partial^2 V}{\partial x_i \partial x_j}$ at the position of the Cu nuclei. The directions can be chosen so that V_{ij} is diagonal. These directions are known as the principal axis of the EFG. Due to Laplace equation ($V_{xx} + V_{yy} + V_{zz} = 0$) the NQR Hamiltonian is determined by only two parameters, ν_q

and η, and is given by

$$\mathcal{H}_q = \frac{\hbar\nu_q}{6}\left[3I_z^2 - \mathbf{I}^2 + \eta\left(I_x^2 - I_y^2\right)\right] \quad (1)$$

where ν_q is a frequency scale proportional to the EFG V_{zz} and

$$\eta = \frac{V_{yy} - V_{xx}}{V_{zz}} \quad (2)$$

is a dimensionless number. It is customary to choose the directions so that $|V_{xx}| \leq |V_{yy}| \leq |V_{zz}|$, and therefore $0 \leq \eta \leq 1$. For the spin 3/2 Cu nuclei this Hamiltonian has only one resonance frequency given by

$$f = \nu_q\sqrt{1 + \frac{\eta^2}{3}}. \quad (3)$$

In $YBCO_7$ and $YBCO_6$ the directions are known experimentally: $\widehat{\mathbf{z}}$ is the $\widehat{\mathbf{c}}$ direction and $\widehat{\mathbf{x}}$ and $\widehat{\mathbf{y}}$ are directions in the CuO_2 plane [7, 8]. In $YBCO_{6.5}$ these directions are determined to be the same on theoretical grounds [8], and are believed not to vary for all other doping [9]. Assuming the directions are doping independent, η is a measure of the local charge homogeneity of the CuO_2 planes. When these planes are homogeneous with local xy rotation symmetry $\eta = 0$. In contrast, when the planes are inhomogeneous due to phase separation as in the case of static stripes, for example, then on the boundary between hole poor and hole rich stripes the xy rotation symmetry will be lost and we expect $\eta \neq 0$. This situation is demonstrated in Fig. 1 obtained using a toy model. The parameters of this model are chosen for clarity only and have no implications on the physical situation in YBCO. A plane of a square lattice with total charge Q is sandwiched between two similar planes with total charge $-Q/2$ each. The electric field produced by each ion is screened with a screening length of two lattice sites. The charge in the central plane is distributed in the form of stripes, 10 atoms wide, and η is numerically calculated. In the figure only the central plane with its stripes, and $|\eta|$ along one line of ions crossing different stripes, are shown. This figure demonstrates that as a result of the stripes $\eta \neq 0$ for all nuclei on the boundary between stripes, despite the fact that the underlying lattice is square. It should be strongly emphasized, however, that we use a stripes-based toy model for the demonstration because of its simplicity, and our experiment has no bearing on the model developed in Ref. [10] where the stripes are dynamic on a time scale much shorter than our experimental one.

Our objective in this work is to determine η as a function of doping in different environments using ADNQR, which is described in detail elsewhere [11]. In this modification of standard NQR one measures the echo intensity in a coil, whose symmetry axis is in the direction

$$\widehat{\mathbf{r}} = (\sin\theta\cos\phi, \sin\theta\sin\phi, \cos\theta)$$

with respect to the principal axis of the EFG, as a function of θ and φ. This situation is demonstrated in the inset of Fig. 2. The echo is obtained using a $\pi/2 - \tau - \pi$ pulse sequence. The pulses are of frequency f, duration $t_{\pi/2}$ and $2t_{\pi/2}$, and create a field $H_1 = \omega_1/\gamma$, where γ is the copper nuclei gyromagnetic ratio. The basic idea behind this experiment is that when $\widehat{\mathbf{r}}$ is in the $\widehat{\mathbf{z}}$ direction, and $\eta = 0$, no spin transitions will occur and no echo will be formed. In contrast when $\eta \neq 0$ an echo will be formed even though $\widehat{\mathbf{r}}$ is parallel to $\widehat{\mathbf{z}}$. For an arbitrary θ and φ the nuclear magnetization M in the coil, at the time of the echo, is given [11, 12] by

$$M(\eta,\theta,\phi) = M_0\lambda\sin^3(\lambda\omega_1 t_{\frac{\pi}{2}}) \quad (4)$$

where

$$\lambda = \frac{1}{2\sqrt{3+\eta^2}}\left\{\left[9 + \eta^2 + 6\eta\cos(2\phi)\right]\sin^2(\theta) + [2\eta\cos(\theta)]^2\right\}^{1/2}, \quad (5)$$

and M_0 is a constant.

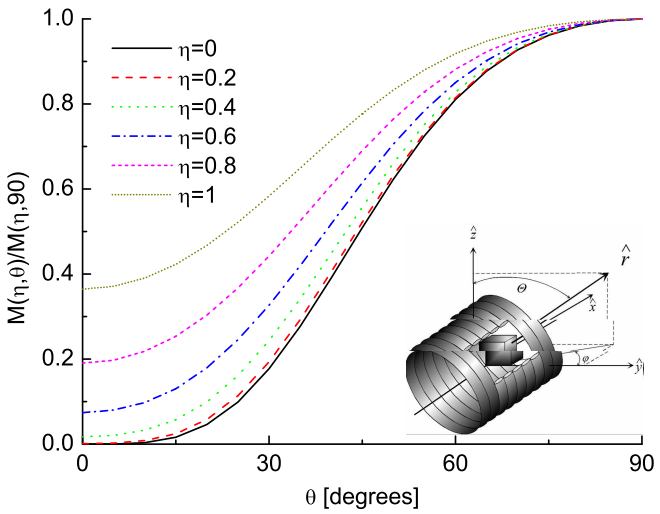

FIG. 2: (Color online) The expected echo intensity for various values of η in an oriented powder (averaged azimuthal angle ϕ) as a function of the polar angle θ between the RF field $\mathbf{H}_1$ and the $\widehat{\mathbf{z}}$ direction of the EFG. The pulse length is optimized at $\theta = 90$ and kept constant throughout the sample rotation. The inset shows the experimental configuration.

We apply the ADNQR experiment to oriented powder of $YBa_2Cu_3O_y$ with $\widehat{\mathbf{c}}||\widehat{\mathbf{z}}$. In such powders the $\widehat{\mathbf{a}}$ and $\widehat{\mathbf{b}}$ directions are mixed. In this case M is obtained from Eq. 4 by averaging over ϕ, namely,

$$M(\eta,\theta) = \frac{1}{2\pi}\int_0^{2\pi}\mathbf{M}(\eta,\theta,\phi)\,d\phi. \quad (6)$$

This averaging must be done numerically, and the expected $M(\eta,\theta)/M(\eta,90)$ for various values of η is presented in Fig 2. The pulse length ($t_{\pi/2}$) is optimized at $\theta = 90$ and is kept constant throughout the rotation of the sample with respect to the coil.

The ADNQR technique has three major strengths: (I) It allows the determination of η even for a wide NQR spectrum and at every point on the spectrum, thus providing a great advantage over nuclear magnetic resonance (NMR), which can determine η only from the entire spectrum with no local resolution; (II) unlike NMR, where one needs to fit the spectrum to 5 different parameters out of which only one is η, ADNQR is sensitive only to η; (III) it allows the determination of η without the application of a static magnetic field and can be used even in the superconducting state. The weakness of ADNQR is that it is very insensitive at small η's as demonstrated in Fig 2.

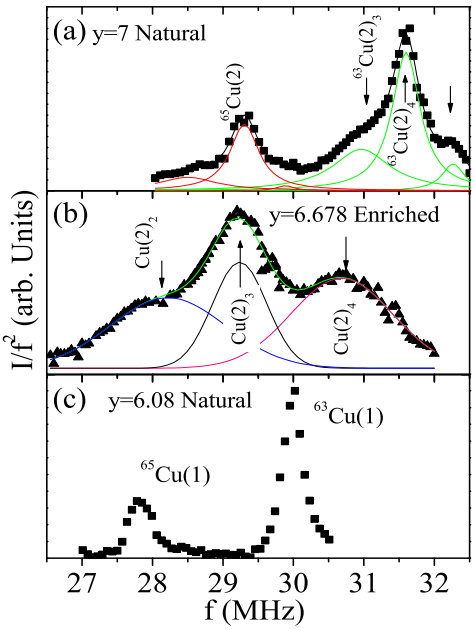

FIG. 3: (Color online) NQR intensities versus frequency f normalized by f^2 in three different $YBCO_y$ samples. The $YBCO_{6.678}$ sample is fully enriched with ^{63}Cu. $YBCO_7$ and $YBCO_{6.08}$ have natural abundance of ^{65}Cu and ^{63}Cu. Also shown are Gaussian fits indicating the contribution to the spectrum of different Cu(2) environments. The arrows show the frequencies where ADNQR is applied.

Before presenting the ADNQR results it is essential to review the NQR frequency assignments in YBCO. In the (a), (b), and (c) panels of Fig. 3 we show the NQR lines at a temperature of 100 K for three different samples with $y = 7.0$, 6.678, 6.08, respectively. The $y = 6.678$ sample is fully enriched with ^{63}Cu. The lines are obtained by a spectrometer with a home-made automated frequency sweep. The echo intensity I is normalized by f^2, where f is the applied frequency, in order to correct for population difference and the induced signal in the coil. The solid lines in Fig. 3 are fits of Gaussians to the data indicating that the spectrum is constructed from contributions of different local environments.

It is simplest to review the enriched $y = 6.678$ spectrum in panel (b) first. This spectrum exhibit three peaks at $f = 28.1$, 29.2, and 30.8 MHz (none of which are from the ^{65}Cu isotope). The peaks are classified in terms of the number of oxygen surrounding the chain copper [Cu(1)] neighboring the detected Cu(2). The higher the oxygen coordination of the this Cu(1), the higher the frequency. In other words, the peak in $f = 30.8$ MHz is from Cu(2) adjacent to a Cu(1) in a fully oxygenated environment [Cu(2)$_4$], the peak in $f = 28.1$ MHz is from Cu(2) nearing a Cu(1) in a fully oxygen deficient environment [Cu(2)$_2$], and finally, the peak in $f = 29.2$ MHz is from Cu(2) whose neighboring Cu(1) is missing one oxygen [Cu(2)$_3$].

The main features in the spectrum of the natural $YBCO_7$ (without enrichment) depicted in panel (a) are two resonance peaks at $f = 31.55$ MHz and $f = 29.3$ MHz. In addition, each peak has two shoulders to the left (31 MHz/28.7 MHz) and right (32 MHz/29.7 MHz) of the biggest peak. The origin of the right shoulder is not clear. The left shoulder is associated again with a partially oxygen deficient environment (mostly Cu(2)$_3$). This spectrum, including the shoulders, resembles the spectrum obtained by others [13, 14], where the lines are identified as the plane-copper isotopes [^{63}Cu(2)] and [^{65}Cu(2)]. The ratio between the peak intensity of the two isotopes is the one expected from their natural abundance, indicating that our spectrometer functions properly.

It is important to mention that the Cu(1) can also contribute intensity to the Cu(2) signal [14]. This is demonstrated in panel (c) for $YBCO_{6.08}$. In this antiferromagnetic sample the Cu(2) signal is at $f = 90$ MHz [15] and in panel (c) only the two isotopes of Cu(1) can be seen [14]. This panel clarifies our careful choice of oxygenation level of the underdoped compound. The Cu(2) peaks of the $y = 6.678$ sample are not contaminated by the Cu(1) signal.

The ADNQR experiments in the $YBCO_7$ sample were done on the ^{63}Cu(2) peak and the two shoulders. In $YBCO_{6.678}$ we investigated the peaks of all different local environments. The frequencies where ADNQR was applied are marked by arrows in panels (a) and (b). The ADNQR experiments were also done at $T = 100$ K temperature using an automated sample rotor. To improve H_1 homogeneity we used a spherical coil.

The ADNQR results for $YBCO_7$ and $YBCO_{6.678}$ in the $\theta = 0$ to 180 range are depicted in Fig. 4. In all cases the intensities at $\theta = 0$ and 180 are lower than at $\theta = 90$, as it should be. It is also clear that the intensity as a func-

tion of angular deviation from $\theta = 90$ drops faster for the $Cu(2)_4$ in both dopings. This is a model-independent observation of the fact that η is smallest for $Cu(2)_4$. The fit of Eq. 6 to the experimental data is demonstrated by the solid lines. In the fit we allow a common finite base line for a given sample, in order to account for some unknown amount of misalignment. We found 24% and 17% misaligned crystallines in the $YBCO_7$ and $YBCO_{6.678}$, respectively. This misalignment is typical. The best fit for $YBCO_7$ peak gives $\eta = 0 \pm 0.15$ in agreement with values previously obtained by NMR for optimally doped YBCO, where the values $\eta = 0$ [16] and $\eta = 0.01 \pm 0.01$ [7] were found. This result reassures us that the experimental method and analysis are correct. Surprisingly, our fit also gives $\eta = 0 \pm 0.15$ for the $Cu(2)_4$ in $YBCO_{6.678}$ sample ($f = 30.8$ MHz). In contrast, in oxygen deficient environments in both $YBCO_7$ and $YBCO_{6.678}$ $\eta \simeq 0.6$. This is the major finding of our work.

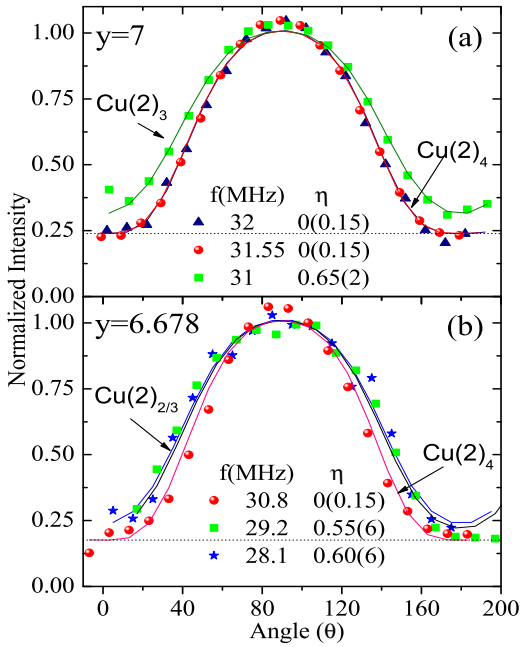

FIG. 4: (Color online) The echo intensity as a function of the angle θ between the RF field $\mathbf{H}_1$ and the principal axis of the electric field gradient $\hat{\mathbf{z}}$ for the two YBCO samples with different oxygen level y, and at three different points in the specturm shown in Fig. 3(a) and (b). The solid lines are fits to Eq. 6 as described in the text.

The data from $YBCO_{6.678}$ are the first evidence for charge anisotropy in such highly doped YBCO. As mentioned before, to date, static charge/spin inhomogeneity has been detected in YBCO by neutron scattering and μSR only up to $y \leq 6.35$ [5, 6]. However, the possibility of electronic phase separation, reflected by $\eta > 0$, is found (within our experimental sensitivity) only in conjunction with quenched disorder. This means that $Cu(2)_4$ cannot reside on a static boundary between two phases of different charge concentration, like the boundary generated by our toy model. This result is in accordance with recent STM measurements [17]. We thus conclude that in YBCO charge inhomogeneity stems from quenched disorder.

We would like to thank H. Alloul, P. Mendels, and J. Bobroff for very helpful discussions. This work was funded by the Israeli Science Foundation and the Posnansky Research Fund in High Temperature superconductivity.

[1] V. J. Emery, S. A. Kivelson, and O. Zachar, Phys. Rev. B **56**, 6120 (1997).
[2] K. M. Lang, V. Madhavan, J. E. Hoffman, E. W. Hudson, H. Eisaki, S. Uchida, J. C. Davis, Nature **415**, 412 (2002). J. E. Hoffman, K. McElroy, D. -H. Lee, K. M. Lang, H. Eisaki, S. Uchida, J. C. Davis , Science **297**, 1148 (2002). M. Vershinin, S. Misra, S. Ono, Y. Abe, Y. Ando, A. Yazdani, Science **303**, 1995 (2004).
[3] Ch. Niedermayer, C. Bernhard, T. Blasius, A. Golnik, A. Moodenbaugh, and J. I. Budnick, Phys. Rev. Lett. **80**, 3843 (1998). C. Panagopoulos, J. L. Tallon, B. D. Rainford, T. Xiang, J. R. Cooper, and C. A. Scott, Phys. Rev. B **66**, 064501 (2002).
[4] P. M. Singer, A. W. Hunt. and T. Imai, Phys. Rev. Lett **88**, 047602 (2002).
[5] H. A. Mook, Pengcheng Dai, and F. Doğan, Phys. Rev. Lett. **88**, 097004 (2002).
[6] S. Sanna, G. Allodi, G. Concas, A. D. Hillier, and R. De Renzi, Rev. Lett. **93**, 207001 (2004).
[7] T. Shimizu, H. Yasuoka, T. Imai, T. Tsuda, T. Takabatake, Y. Nakazawa and M. Ishikawa, Journal of the Physical Society of Japan, **57**, 2494 (1988).
[8] K. Schwarz, C. Ambrosch-Draxl, and P. Blaha, Phys. Rev. B **42**, 2051 (1990).
[9] J. Haase, O. P. Sushkov, P. Horsch, and G. V. M. Williams, Phys. Rev. B **69**, 094504 (2004).
[10] S. A. Kivelson, I. P. Bindloss, E. Fradkin, V. Oganesyan, J. M. Tranquada, A. Kapitulnik, C. Howald, Rev. Mod. Phys. **75**, 1201 (2003).
[11] S. Levy and A. Keren, Journal Magnetic Resonance **167**, 317 (2004).
[12] J. C. Pratt, Molecular Physics, 1977, Vol. 34, No. 2, 539-555.
[13] A. J. Vega, W. E. Farneth, E. M. McCarron, R. K. Bordia, Phys. Rev. B **39**, 2322 (1989).
[14] H. Yasuoka, S. Sasaki, T. Imai, T. Shimizu, Y. Ueda and K. Kosuge ,Phase Transitions **15**, 183 (1989).
[15] H. Yasuoka T. Shimizu, Y. Ueda1 and K. Kosuge1, Journal of the Physical Society of Japan, **57**, 2659 (1988).
[16] C. H. Pennington, D. J. Durand, D. B. Zax, C. P. Slichter, J. P. Rice, and D. M. Ginsberg, Phys. Rev. B **37**, R7944 (1988). H. Lutgemeier, Physica C **153-155**, 731 (1988).
[17] K. McElroy, J. Lee, J. A. Slezak, D. -H. Lee, H. Eisaki, S. Uchida, J. C. Davis, Science **309**, 1048 (2005).